Design Nomograms for Metallic Rocket Motor Cases Reinforced with a Viscoelastic Fiber Overwind

A. Groves* and J. Margetson†
Ministry of Defence, Royal Armament Research and Development Establishment, Westcott, England
and
P. Stanley‡
Simon Engineering Laboratories, University of Manchester, Manchester, England

Two simple graphical design aids are presented depicting the long-time behavior of a prestrained metallic cylinder reinforced with a viscoelastic fiber overwind subjected to uniform internal pressure following complete fiber relaxation. These aids, developed originally for rocket motor case applications, are nevertheless of general relevance and permit the determination of the yield initiation pressure and the winding condition which ensures the maximum yield initiation pressure. Design examples are given with each design aid and their accuracy is demonstrated by comparing the graphically derived results with exact numerical values.

Introduction

MATERIAL selection constitutes an important aspect of rocket motor case design. The minimization of component weight requires that the materials selected exhibit high specific strengths. This has traditionally been achieved by the use of high-strength steels. More recently, however, hybrid rocket motor cases, consisting of a light-weight alloy case circumferentially reinforced with a high-strength polyamide fiber (see Fig. 1), have been considered, since they can be constructed with specific strengths greater than those obained from any steel. Furthermore, if the fiber overwind is applied under tension, a compressive stress is induced in the metallic case, thereby permitting a higher operating pressure before yield.

The design of such motors has received much attention both from the authors[1-5] and other investigators[6,7]. This has involved analyses of the initial winding process, the effects of temperature excursions about the ambient winding temperature, the response of the motor when subjected to its firing pressure, and the influence of fiber viscoelastic relaxation. These analyses have developed stress solutions in closed-form, but experience has shown that the influence of the design variables on the solution cannot always be readily identified without recourse to repetitive computations. To resolve this problem and, more importantly, to provide both a rapid visual representation of the effects of changes in the principal design variables and a clear indication of possible optimum configurations, a series of simple design charts have been developed[8]. These design charts, which are concerned with the determination of the pressure for the initiation of yield in the metallic case, an optimization analysis and the evaluation of the maximum fiber stress, are valid for linear elastic deformations only. The effects of fiber viscoelastic relaxation on the initial case prestress and the subsequent yield pressure behavior of the motor were not considered.

Received Feb. 24, 1986; revision received Sept. 15, 1986.

*Research Scientist.

The purpose of this paper is to develop additional design charts, using as a basis work derived in Ref. 4, to take into account the effects of fiber viscoelastic relaxation on both the yield initiation pressure and the optimization analysis. For the fiber overwind it can be shown that the maximum stress occurs immediately after winding; this stress is obtained directly from the elastic analysis presented nomographically in Ref. 8 and is not further discussed in this paper. For the case, the prestress diminishes with time as the overwind relaxes viscoelastically, and this will affect the pressure necessary for the onset of yield. Because of analytical complexities it is only possible to develop nomographic solutions for the fully relaxed condition. For solutions at intermediate times before complete fiber relaxation, numerical techniques[4] must be employed.

Nomograms are presented for the cylindrical portion of the motor subjected to a uniform internal pressure. During the very brief period of pressure application, viscoelastic relaxation effects may be neglected[4]. Stresses after the pressure application are not considered. The treatment of the geometrically complex regions, e.g., the nozzle region and head end of the motor, which are clearly important, requires numerical or experimental[5-7] studies, the results of which cannot be presented nomographically.

It should be noted that the nucleus of the work presented herein is detailed in Refs. 4 and 8 and, therefore, only the essential design equations are presented. As in Ref. 8, in the derivations of the charts presented, the Poisson's ratio term is taken as 0.33.

II. Yield Initial Predictions

In the design of rocket motor cases, it is a requirement that the motor must withstand all operational loads without failure or excessive distortion. While aeroheat and inertia effects may be present, the predominant load will usually be the firing pressure. To satisfy these requirements and, moreover, to provide acceptable margins of safety one approach is to restrict the operating pressure so that no plastic deformation occurs under maximum load. Although such a definition does not take into account the strength reserves available in the case after the initiation of yield, this definition for the "design" pressure will be adopted in this present treatment.

If it is assumed, as in Ref. 8, that the condition for the initiation of yield in the metallic case is satisfied when the von Mises effective stress is numerically equal to the yield stress in

uniaxial tension[9], then it can be deduced from Refs. 4 and 8 that the pressure for the onset of yield, P_y, at the instant of load application following complete fiber relaxation can be obtained from the quadratic

$$\hat{P}_y^2(4/3)(1-\phi+\phi^2)+\hat{P}_y(2/\sqrt{3})\hat{\sigma}_{\theta w}(\infty)(2\phi-1)+\hat{\sigma}_{\theta w}(\infty)^2-1=0 \quad (1)$$

where

$$\hat{P}_y=P_y/P_{y\max}=\sqrt{3}P_yR\lambda/4t_c\sigma_y$$

$$\phi=[2+(\beta\lambda/3)]/[\lambda(1+\beta)]$$

$$\beta=A_n,\quad \lambda=1-R_e^2/R^2,\quad A=E_f(0)t_f/E_ct_c \quad (2)$$

The quantity $\hat{\sigma}_{\theta w}(\infty)$ is the prestress induced by winding in the case following complete fiber relaxation, nondimensionalized with respect to the yield stress of the metallic case σ_y; it is given by

$$\hat{\sigma}_{\theta w}(\infty)=\sigma_{\theta w}/\sigma_y=-\psi_w\ell n(1+\beta)\left\{\frac{1+\beta}{1/\alpha+\beta}\right\} \quad (3)$$

with ψ_w and α denoting, respectively,

$$\psi_w=E_c\epsilon_w/\sigma_y$$

$$\alpha=E_f(\infty)/E_f(0) \quad (4)$$

In Eqs. (3) and (4) E_c is the Young's modulus for the case, $E_f(0)$ and $E_f(\infty)$ are respectively the short- and long-time moduli of the fiber, t_c is the case wall thickness and t_f is the effective thickness of a single fiber layer (a submultiple of the actual fiber thickness to take into account fiber packing). The term R_e is the effective nozzle insert radius, calculated to allow for the effects of inertia; the variable R denotes the mean cylinder radius and n the number of applied fiber layers. The initial winding strain is denoted by ϵ_w and $P_{y\max}$ is the maximum attainable yield initiation pressure for a circumferentially reinforced motor,[2] i.e.,

$$P_{y\max}=4t_c\sigma_y/\sqrt{3}R\lambda \quad (5)$$

The minimum positive root of Eq. (1) is taken as the nondimensional yield initiation pressure $\hat{P}_y$, with P_y then following from Eqs. (2).

A solution to Eq. (1), and more importantly a visual appreciation of the influence of the principal variables on the yield initiation pressure, can now be obtained from the simple design chart derived from Eq. (1) and given in Fig. 2. As in Ref. 8, the ranges of the variables used in this and the subsequent figures (see Table 1) are typical of overwound rocket motor cases, but these can be readily changed to satisfy the problem under consideration.

The use of the design chart necessitates a knowledge of four of the five variables appearing in it, i.e., ψ_w, $\hat{P}_y$, α, λ and β. Any one of the first four can be readily "read" from the figure (i.e., ψ_w, $\hat{P}_y$, α, and λ) in terms of the remaining four but, as in Ref. 8, difficulties arise with β, due to its appearance on two of the graduated scales. In principle a trial-and-error solution procedure for β is possible, but in practice a more simple approach is to specify the nondimensional case prestress following complete fiber relaxation, $\hat{\sigma}_{\theta w}(\infty)$, so that the solution procedure follows in a manner similar to that detailed in Ref. 8.

To illustrate the use of the chart, the yield initiation pressure following complete fiber relaxation is evaluated for a sample motor case[2,4,8], in terms of ψ_w, λ, α, and β (see Table 3) derived from the details given in Table 2. Evaluation can be obtained as follows:

1) Using the left-hand side of the figure locate a point within the $\alpha-\beta$ grid corresponding to $\alpha=0.5$ and $\beta=1.82$. Project this point horizontally to intersect the right-hand edge of the $\alpha-\beta$ grid.

2) From the intersection obtained in 1) construct a straight line to pass through $\psi_w=0.22$ to intersect the $\hat{\sigma}_{\theta w}(\infty)$ scale as indicated in Fig. 2.

Table 1 Typical ranges of nondimensional variables

	Values	
	Min	Max
Nondimensional winding parameter, ψ_w	0	2.0
Nondimensional fully relaxed case prestress, $\hat{\sigma}_{\theta w}(\infty)$	0	−1
Nondimensional yield initiation pressure, $\hat{P}_y$	0	1.0
Radius parameter, λ	0	1.0
Stiffness parameter, β	0	5.0
Fiber viscoelastic modulus ratio, α	0	1.0

Table 2 Sample motor case

Fiber moduli	
Short-time, $E_f(0)$	124 GPa
Long-time, $E_f(\infty)$	62 GPa
Young's modulus, E_c	70 GPa
Yield stress, σ_y	470 MPa
Thicknesses	
Fiber (effective), t_f	0.1 mm
Case, t_c	1.95 mm
Radii	
Motor, R	46.0 mm
Throat insert (effective), R_e	32.53 mm
Winding strain, ϵ_w	1.5×10^{-3}
No. of layers, n	20

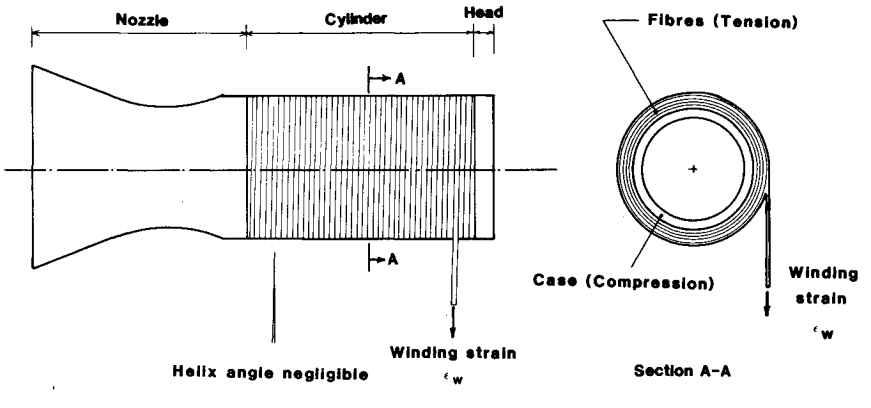

Fig. 1 Schematic of a metallic rocket motor case circumferentially reinforced with a fiber overwind.

3) Using the lower right-hand portion of the chart construct a second straight line, in this case, to pass through $\beta = 1.82$ and $\lambda = 0.5$. Mark the intersection of this line with the ϕ scale.

4) Project two lines, the first horizontally, the second vertically, across the $\hat{\sigma}_{\theta w}(\infty) - \phi$ grid from the intersections obtained in 2) and 3), respectively.

5) Evaluate the $\hat{P}_y$ value corresponding to the intersection of the lines drawn in 4) and thence P_y from Eqs. (2).

For the example considered, Fig. 2 gives a yield initiation pressure of 63.0 MPa. This is in good agreement with the numerical value of 62.4 MPa. It is important to note that the short-time (i.e., the instantaneous elastic) solution can also be obtained from Fig. 2 by setting $\alpha = E_f(\infty)/E_f(0) = 1$; the value obtained is 67.2 MPa.

Having obtained both the long- and short-time yield initiation pressures the influence of fiber viscoelastic relaxation can be quantitatively assessed. A decrease of 6.5% has occurred in this example. It should be noted, however, that this decreasing trend may not always be observed. Recent work[4] has shown that, depending on the initial winding conditions, the yield pressure can increase, decrease, or increase to a maximum and then decrease with fiber relaxation. Nevertheless, the maximum attainable yield initiation pressure will always be given by Eq. (5).

An insight into which of these three yield pressure trends a motor will follow can be obtained from Fig. 2. Points representing the short- and the long-time solutions are readily located in the figure. The latter will always be "vertically" below the former. If both points are to be left of the $\hat{P}_y = 1$ curve, then the yield initiation pressure will increase with fiber relaxation, whereas if both points are to the right, the opposite is true. Moreover, if the short-time point is to the left of the curve and the long-time point to the right, then the yield pressure will increase to the maximum attainable value [given by Eq. (5)] and then decrease with fiber relaxation. These trends may have some relevance in service life prediction studies.

As a further illustration of the trends embodied in Fig. 2, the variation of the yield pressure as a function of the number of applied fiber layers has also been studied in detail for the Table 2 motor. The results of this study are shown in Fig. 3, where the short- and long-time versions of this variation for two typical initial winding strain values of 3.0×10^{-3} and 4.5×10^{-3} are plotted. It is evident from the figure that there is a unique number of fiber layers, for a given winding strain, for which the short- and long-time yield pressure values coincide. For smaller numbers of fiber layers the effect of fiber relaxation is to reduce the yield pressure, and vice versa.

III. Optimization Analysis

For fiber-reinforced metallic rocket motor cases an optimum configuration has been identified which corresponds to the maximum attainable yield initiation pressure for overwound motors. Assuming the von Mises yield criterion this maximum is given by Eq. (5) and is independent of the winding strain, the number of applied fiber layers and the physical properties of the fiber. Nevertheless, as shown in Fig. 3, the number of layers required to achieve this maximum is dependent on both the magnitude of the winding strain and the degree of fiber relaxation which takes place. After some manipulation, it can be shown from Refs. 2 and 4 that the governing relationship between these variables is

$$\left\{\frac{4}{\lambda} - 1 - \frac{\beta}{3}\right\}\frac{1}{1+\beta} = \sqrt{3}\psi_w \ell n(1+\beta)\left\{\frac{1+\beta}{1/\alpha+\beta}\right\} \tag{6}$$

Table 3 Derived variables for motor case in Table 2

Nondimensional winding parameter, ψ_w	0.22
Radius parameter, λ	0.5
Stiffness parameter, β	1.82
Fiber viscoelastic modulus ratio, α	0.5

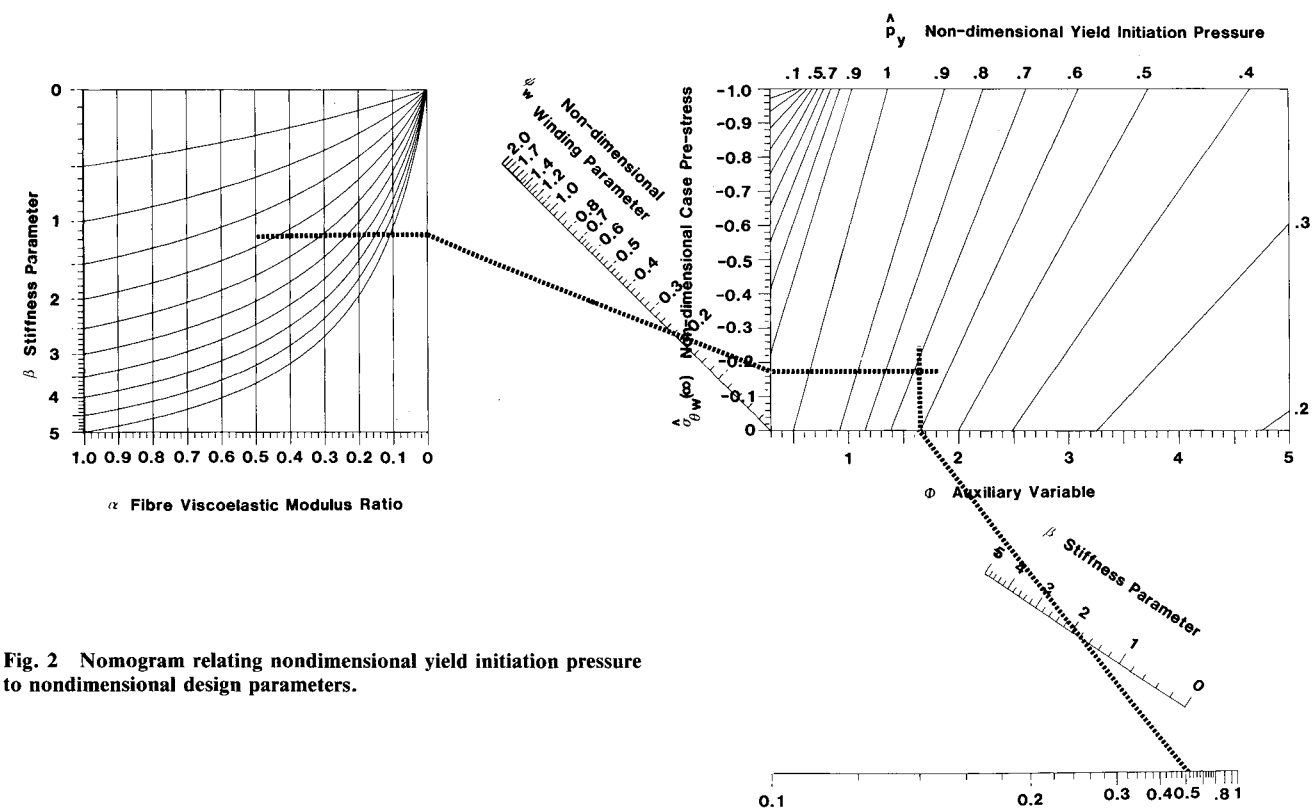

Fig. 2 Nomogram relating nondimensional yield initiation pressure to nondimensional design parameters.

Because of the simplicity of the nomogram and, moreover, because each variable is uniquely defined by a single graduated scale, any one of the four variables can be readily obtained in terms of the other three. In order to determine the winding strain necessary to obtain the optimum configuration following complete fiber relaxation for the Table 2 motor in terms of the derived variables α, β, and λ (see Table 3), the nomogram is used as follows:

where λ and β are defined by Eqs. (2) and ψ_w and α by Eqs. (4).

As with the elastic optimization nomogram,[8] for a prescribed n value Eq. (6) can be readily solved for the optimum winding strain but the determination of the optimum number of fiber layers for a prescribed winding strain would generally require computer assistance. Alternatively, the optimization nomogram derived from Eq. (6) and shown in Fig. 4 can be used.

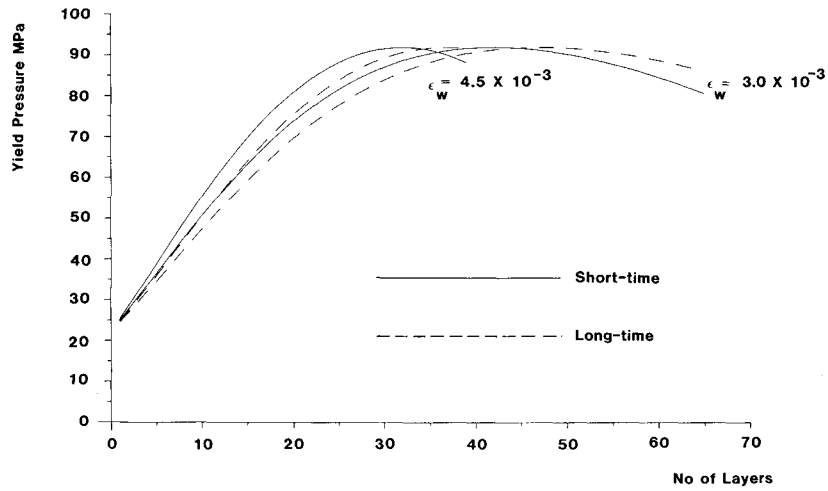

Fig. 3 Variation of short- and long-time yield initiation pressures with number of applied fiber layers for two typical winding strains.

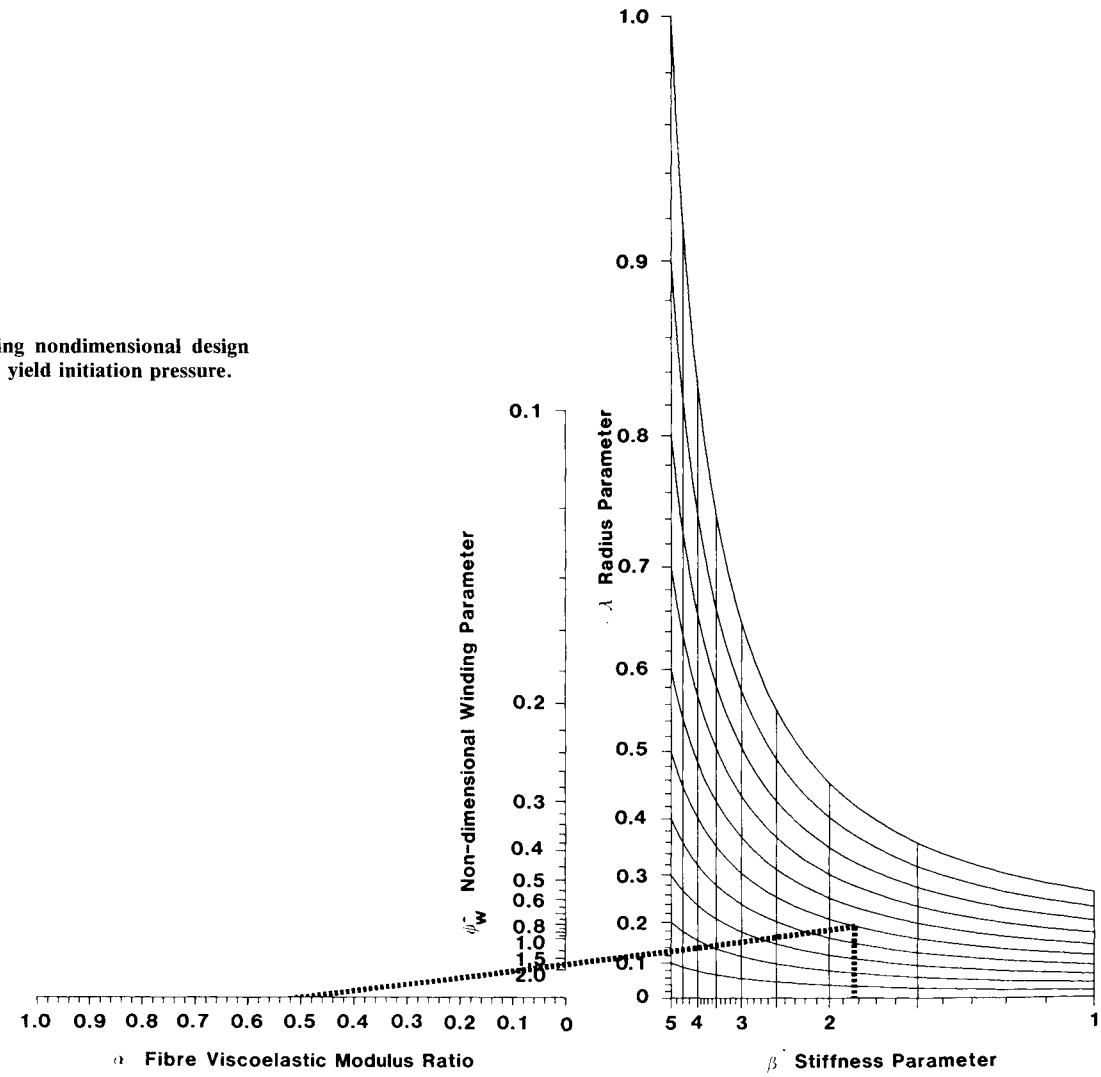

Fig. 4 Nomogram relating nondimensional design parameters for maximum yield initiation pressure.

1) Locate a point within the $\beta-\lambda$ grid corresponding to the intersection of $\beta=1.82$ and $\lambda=0.5$.

2) From this point draw a straight line to pass through 0.5 on the α scale to obtain the required ψ_w value as shown.

Having determined ψ_w, the optimum winding strain follows from Eqs. (4). In this example the nomogram gives an optimum winding strain of 1.17×10^{-2} which compares favorably with the numerical value of 1.15×10^{-2}. This is some 38% greater than that required for the elastic analysis.[8] The maximum yield initiation pressure of 92.0 MPa corresponding to this optimum is calculated from Eq. (5). The importance of achieving the optimum configuration can be judged from the fact that this value is 46.0% greater than that obtained for the arbitrary configuration considered in Sec. 2.

Although the foregoing technique provides a simple and concise method for determining the optimum winding configuration, it should be noted, however, that the Fig. 4. nomogram makes no attempt to assess whether the metallic case can support the initial prestress without yielding in compression. To check for this condition it becomes necessary to use the optimized design variables in conjunction with the Fig. 2 nomogram to determine the magnitude of the nondimensional prestress $\hat{\sigma}_{\theta w}(\infty)$. Clearly, if this value exceeds -1, i.e., $|\hat{\sigma}_{\theta w}(\infty)|>\sigma_y$ (as is the situation in this illustrative example), the case will deform plastically during winding, indicating that the foregoing analysis is void and, moreover, that an optimized configuration cannot be achieved. As a further illustration, if a β value of 4 is selected, necessitating an optimum winding strain of 3.36×10^{-3}, it can be easily established from Fig. 2 that for this revised β value that the nondimensional prestress is now less than -1 (-0.67). Consequently, an optimized motor can be obtained. This, in turn, can be further verified by completing the Fig. 2. nomogram to confirm that the resulting nondimensional yield initiation pressure $\hat{P}_y=1$.

4 Conclusions

Two simple graphical design aids have been presented depicting the influence of fiber viscoelastic relaxation on the long-time behavior of a metallic cylinder reinforced with a viscoelastic fiber overwind. These charts, which complement elastic design charts developed in a previous publication, have been developed specifically for rocket motor applications, but they are nevertheless equally valid for any fiber-reinforced cylinder subjected to an instantaneous pressure application following complete fiber relaxation. The charts presented permit the determination of: 1) the pressure for the initiation of yield in the metallic case in terms of the principal variables, i.e., the winding strain, the material properties, the number of layers; and 2) the combination of design variables which ensures that the maximum yield initiation pressure is attained.

Examples have been presented for both design charts and their accuracy demonstrated by comparing the graphically derived results with exact numerical solutions.

References

[1]Groves, A., Margetson, J., and Stanley, P., "Stress Analysis of Fibre-Reinforced Metallic Rocket Motor Cases." Ministry of Defence (PE) Rept.

[2]Stanley, P., Margetson, J., and Groves, A., "Analytical Stress Solutions for Fibre-Reinforced Metallic Rocket Motor Cases," *International Journal of Mechanical Science*, Vol. 26, 1984, pp. 119–130.

[3]Margetson, J., "Stress Analysis Procedures for the Design of Fibre-Reinforced Metallic Rocket Motor Cases," AIAA Paper 83–1330, June 1983.

[4]Margetson, J., Groves, A., and Stanley, P., "Stress Analysis of Metallic Rocket Motor Cases Reinforced with a Viscoelastic Fibre Overwind," *International Journal of Mechanical Science*, Vol. 27, 1984, pp. 439–452.

[5]Margetson, J. and Groves, A., "Structural Analysis of Fibre-Reinforced Metallic Rocket Motor Cases using Finite Element and Photoelastic Techniques," Ministry of Defence (PE) Rept (not published).

[6]Cook, J., Unpublished Ministry of Defence (PE) Repts.

[7]Parratt, N. J., Unpublished Ministry of Defence (PE) Repts.

[8]Groves, A., Margetson, J., and Stanley, P., "Nomographic Design Procedures for Fibre-Reinforced Metallic Rocket Motor Cases," *Journal of Strain Analyses*, Vol. 21, 1986, pp. 146–151.

[9]Mendelson, A., *Plasticity: Theory and Application*, 1st ed., Macmillan, New York, 1968.